Microscale modeling of kinking nonlinear elastic solids

M. W. Barsoum, T. Zhen, A. Zhou, S. Basu, and S. R. Kalidindi
Department of Materials Science and Engineering, Drexel University, Philadelphia, Pennsylvania 19104, USA
(Received 3 September 2004; revised manuscript received 24 November 2004; published 4 April 2005)

Recently we identified and classified a class of solids as kinking nonlinear elastic (KNE) because they deform by the formation of kink bands. KNE solids represent a large family that include, among others, layered ternary carbides and nitrides, layered oxides and semiconductors, zinc, cadmium, graphite, ice, and the layered silicates, such as mica, present in nonlinear mesoscopic elastic solids. Herein we present a microscale model that accounts for the mechanical response of KNE solids to compressive stresses and apply it to two very different solids: Ti_3SiC_2 and graphite. Building on the Frank and Stroh model put forth in the 1950's for the formation of kink bands, we developed a comprehensive theory that accounts for the contributions of incipient kink bands (IKBs) and dislocations pile-ups produced by normal glide processes to the nonlinear strains and stored strain energies. The theory provides estimates for the densities of IKBs, the dislocation densities, both from the IKBs and dislocation pileups, as well as the energy dissipated by the motion of the dislocations.

DOI: 10.1103/PhysRevB.71.134101 PACS number(s): 62.20.−x

I. INTRODUCTION

In recent papers,[1–4] we have shown that the *MAX* phases, mica, graphite, hexagonal BN and most probably ice, can be classified as kinking nonlinear elastic (KNE) solids. The *MAX* phases are a new class of layered, machinable, ternary carbides, and nitrides, with the chemical formula $M_{n+1}AX_n$, where M is an early transition metal, A is an A-group element (mostly IIIA and IVA) and X is C or N. A prime example of the *MAX* phases is Ti_3SiC_2, the properties of which have been extensively studied.[1,2,5–17] We also believe that many of the so-called nonlinear mesoscopic elastic (NME) solids discussed in the geological literature[18–23] are in fact KNE solids.[3] All KNE solids deform primarily by kinking and the formation of kink bands (KBs). We have shown that kinking—a mechanism first reported by Orowan[24] in single crystals of Cd loaded parallel to the basal planes—is the physical origin of the hysteretic, nonlinear elastic, behavior exhibited by these solids.[3]

The loading-unloading stress-strain curves of KNE solids in the elastic regime outline nonlinear, fully reversible, reproducible, closed hysteresis loops whose shape and extent of energy dissipated are strongly influenced by grain size, with the energy dissipated being significantly larger in the coarse-grained material.[1] The response is nonlinear and hysteretic (Fig. 1). In prior studies,[1–4] we attributed these unique characteristics to the formation and annihilation of incipient kink bands (IKBs). Incipient and regular KBs have also been held responsible for the fully reversible and hardening behavior of KNE solids as diverse as graphite and mica indented with spherical indenter at the nanolength scales.[2–4]

KNE solids are characterized by a marked anisotropy in their plastic properties at the single crystal level. They do not twin, but deform by kinking. We thus postulated that a sufficient, but not necessary, condition for a solid to be a KNE is a high c/a ratio[3]. If c/a is not high then, the solid should have a low c_{44}. In recent papers[1–4] it has been emphasized that the formation of IKBs must precede the production of regular KBs. IKBs are made up of near parallel walls of opposite sign dislocations that are undissociated, i.e., still attracted to each other at the ends [Figs. 2(a) and 2(b)]. They annihilate when the load is removed. When IKBs dissociate, they produce mobile dislocation walls (MDWs), and hence irreversible or permanent deformation [Fig. 2(c)] and damage in the form of delaminations. It is the coalescence of mobile walls that eventually produces the kink boundaries that result in KBs [Fig. 2(d)] that have been documented extensively in the literature.[5–8,21–26]

In this paper, we present our efforts to develop a microscale model for the mechanical response of KNE solids. We applied the model to Ti_3SiC_2 and graphite, two vastly differently bonded solids.

II. MICROSCALE CONSIDERATIONS

The total strain ε_{tot} can be additively decomposed into a linear elastic strain and a nonlinear strain ε_{NL}:

$$\varepsilon_{tot} = \frac{\sigma}{E} + \varepsilon_{NL} = \frac{\sigma}{E} + \varepsilon_{IKB} + \varepsilon_{DP}, \tag{1}$$

where σ/E represents the linear elastic component, where E denotes the Young's modulus of the material and σ the uniaxial applied stress. In the most general case, and in the absence of phase transitions and/or microcracking, the nonlinear fully reversible strain ε_{NL} is comprised of two components. The first ε_{IKB} is due to IKBs and the second—due to basal slip that leads to dislocation pileups (DPs)—is denoted as ε_{DP}. Note here that because of the layered nature of KNEs both strains are fully reversible. In what follows each will be dealt with separately.

At this juncture it is worth noting that in general the response of KNE solids to cyclic stress is one of two types. Type I is one in which the first and all subsequent cycles to the same stress are fully reversible [Fig. 1(a)]. Type II response is one in which the first cycle is slightly open—i.e., results in a permanent deformation—but all subsequent cycles to the same stress are fully reversible [Fig. 1(b)]. The response of the *MAX* phases is of type I; that of graphite and

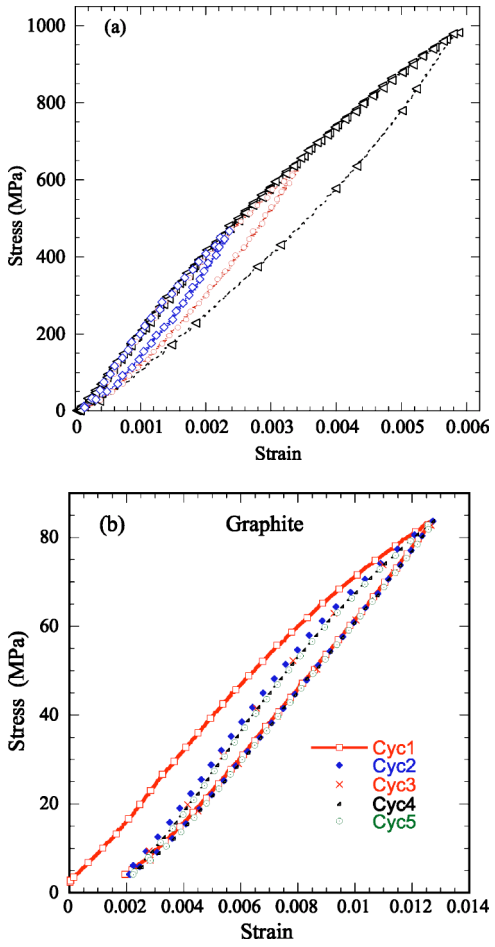

FIG. 1. (Color online) Typical stress-strain curves of KNE solids, (a) Ti_3SiC_2 which is of type I and (b) graphite, which is of type II.

hexagonal BN for example, is of type II. The reason for the differences in response is unclear at this time, but may be related to the ease of delaminations and/or weak grain boundaries in type II solids. This comment notwithstanding more work is needed to understand the differences. These distinctions, however, are not important to this work for two reasons: We only model the *fully reversible* response, and the permanent strains recorded in the first cycles are usually quite small.

Herein we seek to establish a relationship between $\varepsilon_{\mathrm{IKB}}$ and $\varepsilon_{\mathrm{DP}}$ and their contributions to the stored nonlinear strain energy per unit volume U_{NL}. The total *stored* strain energy U is defined as the *total* mechanical energy input into the system during a *loading* sequence minus the energy dissipated due to internal friction as a result of dislocation motion. For a monotonic loading segment, it follows that

$$U = W - \frac{W_d}{2} = U_{\mathrm{LE}} + U_{\mathrm{IKB}} + U_{\mathrm{DP}},$$

where W represents the total mechanical energy input into the system (total area under the measured stress-strain curve), W_d is the energy dissipated in a complete loading-unloading cycle, U_{LE} is the stored energy component from

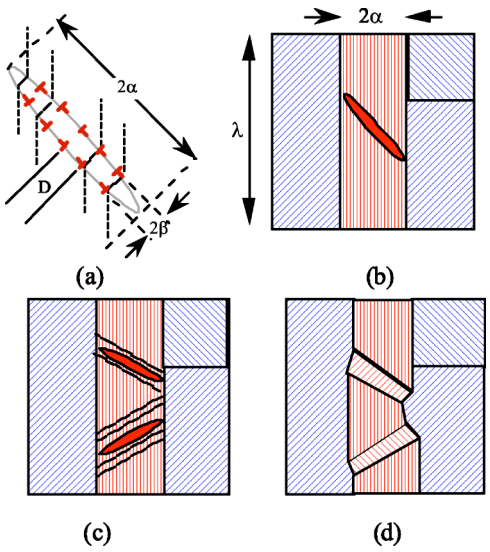

FIG. 2. (Color online) Schematic description of the formation of a kink band. (a) A thin elliptical subcritical kink nucleus is formed with $2\alpha \gg 2\beta$. The boundaries are comprised of dislocation walls (shown in red) of opposite sign, and a uniform spacing of D. (b) Formation of an IKB in hard (red) grains adjacent to soft (blue) grains. The lines in the grains denote basal planes. An IKB is fully reversible upon the removal of the load. (c) Mobile dislocation walls formed by the sundering of IKBs. Solid inclined lines denote walls that have separated from the source and are moving away from it. This only happens at higher temperatures and/or high stresses. (d) Same as (c) but after removal of stress, emphasizing formation of permanent kink boundaries that are indistinguishable from grain boundaries. These KBs, in effect, reduce the domain size and result in hardening.

linear elasticity, arising from stretching of atomic bonds, and U_{IKB} and U_{DP} are the stored energy components from IKBs and DPs, respectively. (Here W_d represents the energy dissipated in a complete loading-unloading cycle, consistent with our earlier papers.[1] The rationale for dividing W_d by two is that approximately half the energy dissipation occurs during loading and half during unloading.) Referring to Fig. 3, it follows that the hatched area represents U_{NL}, where

$$U_{\mathrm{NL}} = U_{\mathrm{IKB}} + U_{\mathrm{DP}}.$$

Note that W_d corresponds to the area enclosed by the hysteresis loops, and is distinct from the definition of U_{NL}. Also note that

$$U_{\mathrm{NL}} = 1/2\sigma\varepsilon_{\mathrm{NL}}. \quad (2)$$

At this juncture it is useful to separate the discussion and address the contributions of the IKBs and the DPs separately. To carry out some of the calculations outlined below, a number of material properties, listed in Table I, are required. The rationale and references for the choices made can be found in the Appendix.

A. Nonlinear elastic strain from IKBs

Frank and Stroh[25] (FS) proposed a model in which pairs of dislocations of opposite sign nucleate and grow as a thin

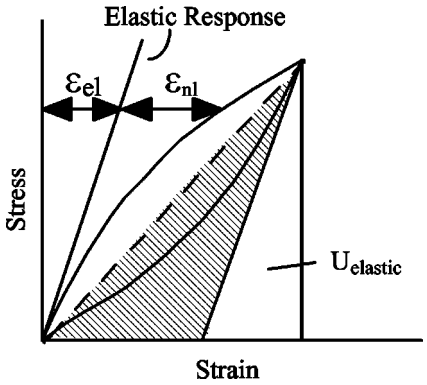

FIG. 3. Schematic of stress-strain curve upon loading. The shaded area represents $U_{NL}=W-\sigma^2/2E-W_d/2$, where W is the total area under the curve and W_d is the energy dissipated per cycle per unit volume. Also shown are the linear ε_{EL} and nonlinear ε_{NL} contributions to the total strain. Note that $U_{NL}=1/2\sigma\varepsilon_{NL}$.

elliptical kink with dimensions 2α and 2β, such that $2\alpha \gg 2\beta$ [Fig. 2(a)]. It has been postulated that a subcritical kink can grow by producing new dislocation pairs at its edges, or conversely shrink by annihilation of dislocation pairs. Specifically, FS derived the following condition for the unstable growth of kinks:

$$\gamma_c = \frac{b}{D} \approx \frac{3\sqrt{3}(1-v)\tau_{loc}}{2G}, \tag{3}$$

where D is the distance between dislocations along 2α [Fig. 2(a)]; γ_c is the critical kinking angle (or shear strain); G and v are the shear modulus and Poisson's ratio, respectively. τ_{loc} is the local shear stress needed to form a dislocation pair; in metals it is usually assumed to be $\approx G/30$. If the same assumption is made here, γ_c is small; it is ≈ 0.07 for Ti_3SiC_2 and ≈ 0.065 for graphite.

The remote shear stress, τ, needed to render a kink nucleus unstable and grow depends on 2α and is given by[25]

$$\tau > \tau_c \approx \frac{\sigma_c}{2} \approx \sqrt{\frac{2bG^2\gamma_c}{\alpha\pi^2}\ln\left(\frac{b}{r\gamma_c}\right)}, \tag{4}$$

where τ_c and σ_c are the critical shear and axial stresses, respectively. r is related to the core energy of the dislocation and is of the same order as the Burgers vector b.[25] Throughout this paper we assume $\tau \approx \sigma/2$. FS modeled pure edge dislocations, which introduces a $(1-v)$ term in the denominator of Eq. (4). This term was omitted here, and in the reminder of this paper, because in Ti_3SiC_2 the dislocations, while perfect, are mixed and self-organize in walls such that the screw components alternate, hence reducing their energy.[6] In graphite the dislocations split into partials, also reducing their energy.[27]

Equation (4) suggests that the stress for kinking decreases with increasing 2α. In reality, 2α is constrained by the thicknesses of the individual grains, or domains in which the kink are being produced (see below). Therefore, once a kink nucleus is formed and the condition for unstable growth is met [Eq. (4)] the kink will grow rapidly until it meets a grain boundary. If the kink remains undissociated at this juncture, we refer to it as an IKB[1] [Fig. 2(b)]. IKBs are fully reversible.[1]

The width of the band, 2β is given by[25]

$$2\beta \approx \frac{2\alpha(1-v)}{2G\gamma_c}\sigma. \tag{5}$$

Assuming the IKBs to be cylinders with radii β the total energy U_{IKB} needed to create N_k kinks per unit volume is given by[25]

$$U_{IKB} = (2\pi\beta N_k)\frac{Gb\alpha\gamma_c}{\pi}\ln\left(\frac{b}{r\gamma_c}\right), \tag{6}$$

where $(Gb\alpha\gamma_c/\pi)\ln(b/r\gamma_c)$ represents the energy per unit length of dislocation line needed to create a kinked region of length 2α.[25] In Eq. (6), for reasons discussed earlier, the $(1-v)$ term in the denominator was omitted.

The strain produced by these kinks is

$$\varepsilon_{IKB} = \frac{2\pi\alpha\beta^2\gamma_c N_k}{k}, \tag{7}$$

where k represents a factor that relates the IKB shear strain at the grain level to the macroscale uniaxial strain. This factor would depend on various microstructural parameters that would control the orientations of the IKBs with respect to the loading axis, e.g., the crystallographic texture in the sample. Here we assume k is equal to 1.

At low stresses, it is reasonable to assume that the internal stress is constant and equal to that given by Eq. (4). Thus combining Eqs. (4)–(7) yields

$$U_{IKB} = \sqrt{\frac{G^2 b\gamma_c}{2\alpha(1-v)^2}\ln\left(\frac{b}{r\gamma_c}\right)}\varepsilon_{IKB}. \tag{8}$$

Note that the term under the square root is essentially σ_c given by Eq. (4). It follows that as long as the applied stress

TABLE I. Summary of material constants and some values calculated herein. See the Appendix for rationale and references. N is the number of loops per IKB.

	G (GPa)	v	b (Å)	r/b	γ_c (rad)	λ (μm)	2α (μm)	σ_c (MPa)	σ_t (MPa)	N
FG	144	0.20	3	11	0.07	8±4	3±1.5	250	216	700
CG						42±39	20±16	130	50	4670
Graphite	4.5	0.25	1.4	11	0.065	0.024[a]	0.023	57	23	10

[a]This value was estimated from the intercept of the line labeled graphite along the x axis and Eq. (11).

is low, then $\sigma \approx \sigma_c$, and Eq. (8) can be used to calculated r, if α is known.

If that assumption is not made, then combining Eqs. (2), (5), and (7) results in

$$U_{\mathrm{IKB}} = \sqrt{\frac{G^2\gamma_c}{2\pi(1-\upsilon)^2 N_k \alpha^3}}\varepsilon_{\mathrm{IKB}}^{1.5}, \tag{9}$$

This relationship—which is valid over the entire loading domain as long as the total nonlinear strain is assumed to be due to IKBs alone—can be used to calculate N_k, again assuming 2α is known. Interestingly at high stresses and/or for very fine-grained solids $N_k\alpha^3$ should be of the order of unity, a fact borne out by the results shown below.

B. Nonlinear elastic strain from dislocation pile-ups

The number of dislocations in a pileup on a single slip plane is given by[28]

$$n \approx \frac{\pi\lambda\tau}{Gb},$$

where λ is the length of the pileup. The presence of N_{DP} pileups per unit volume, will result in a strain of

$$\varepsilon_{\mathrm{DP}} = nN_{\mathrm{DP}}\lambda^2 b. \tag{10}$$

Using this equation and assuming the energy required to produce one dislocation loop per unit length of dislocation line is $\approx Gb^2/2$ it follows that

$$U_{\mathrm{DP}} = \frac{\pi Gb}{2\lambda}\varepsilon_{\mathrm{DP}}. \tag{11}$$

In deriving this equation the length of the average dislocation loop was assumed to be $2\pi\lambda/2$. In this paper, λ is the grain diameter [Fig. 2(b)].

Combining Eqs. (8) and (11) the following relationship, only valid at lower stresses, is obtained:

$$U_{\mathrm{NL}} = \frac{\pi Gb}{2\lambda}\varepsilon_{\mathrm{DP}} + \sqrt{\frac{G^2 b\gamma_c}{2\alpha(1-\upsilon)^2}\ln\left(\frac{b}{r\gamma_c}\right)}\varepsilon_{\mathrm{IKB}}. \tag{12}$$

Similarly combining Eqs. (9) and (11) one obtains the relationship

$$U_{\mathrm{NL}} \approx \frac{\pi Gb}{2\lambda}\varepsilon_{\mathrm{DP}} + \sqrt{\frac{G^2\gamma_c}{2\pi(1-\upsilon)^2 N_k\alpha^3}}\varepsilon_{\mathrm{IKB}}^{1.5} \tag{13}$$

that should be valid over the *entire* stress regime. As discussed below, for most KNE solids with grain sizes greater than ≈ 1 μm, the first term can be ignored relative to the second term and Eq. (13) can then be rewritten as

$$U_{\mathrm{NL}} \approx \sqrt{\frac{G^2\gamma_c}{2\pi(1-\upsilon)^2 N_k\alpha^3}}(\varepsilon_{\mathrm{NL}} - \varepsilon_{\mathrm{DP}})^{1.5}. \tag{14}$$

C. Experimental data and analysis

From our experiments[1,4] we can readily measure U_{NL}, as a function of $\varepsilon_{\mathrm{NL}}$. The results for graphite, fine-grained and coarse-grained Ti_3SiC_2 are shown in Fig. 4(a).

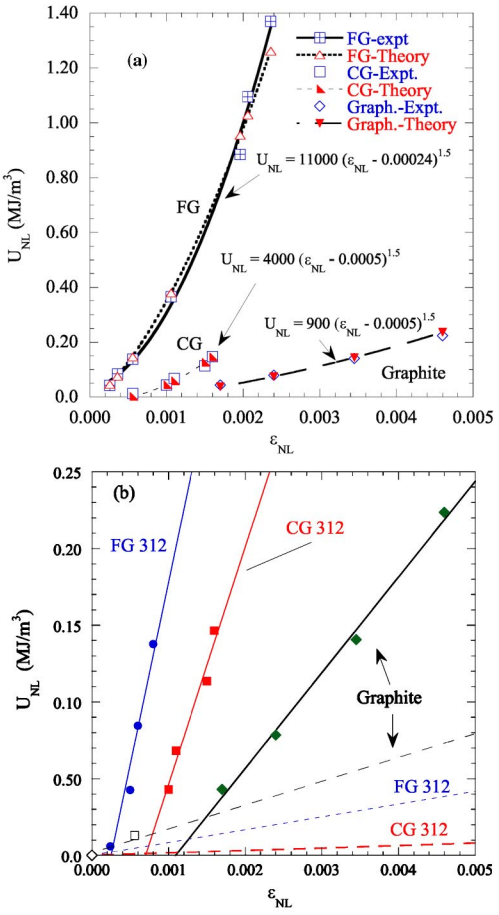

FIG. 4. (Color online) (a) Plot of U_{NL} versus $\varepsilon_{\mathrm{NL}}$ for the three materials tested herein. The prefactors and strain shifts, presumably due to DPs, needed to obtain the best agreement between theory and experiment are shown in the form of an equation, where the exponent on the strain term was fixed at 1.5. (b) Same as (a), but emphasis on low strain corner. Dashed lines represent the first term on the right hand side of Eq. (12), assuming λ is the grain diameter. Solid lines are least squares fits of the low stress results from which r is calculated for the FG microstructure [viz. from second term of Eq. (12)].

Given that KNE solids possess less than the five independent slip systems needed for ductility, initially upon loading DPs occur in grains oriented favorably for basal slip, the so-called soft grains. With increasing stress, there is a buildup of large internal stresses[10,14,17,29] and kinking is initiated in the hard grains. To simplify the discussion, we assume these mechanisms occur sequentially and consider two regimes; a low σ regime where Eq. (12) is valid, and a second regime where Eq. (13) is. Each is treated separately below.

1. Low stress regime

The dashed lines in Fig. 4(b) represent the first term in Eq. (12) based on the values listed in Table I, i.e., assuming λ, to be the average grain diameter. In the case of Ti_3SiC_2 it is obvious that the contribution of the dislocation pileups to

TABLE II. Summary of experimental results and calculations. Note in these calculations the 2α values used for the FG and CG Ti_3SiC_2 were 3 and 11 μm, respectively. N_{IKB} was calculated from Eq. (7), assuming β is given by Eq. (5). The average distance between IKBs, $d_{IKB} \approx (N_{IKB})^{-1/3}$, is listed in the last column.

Solid	σ (MPa)	2β (μm)	ε_{IKB}	U (MJ/m^3)	W_d (MJ/m^3)	N_K $(\mu m)^{-3}$	δ (μm)
Ti_3SiC_2 FG	105	0.012	0.00024	0.007	0.0023	9.3[a]	≈ 1 assuming $N_{IKB}=1\times10^{18}$ m^{-3}
	260	0.03	0.0005	0.053	0.021	3.2[a]	
	365	0.043	0.0006	0.112	0.055	1.9	
	470	0.056	0.0008	0.20	0.12	1.5	
	625	0.074	0.0013	0.49	0.24	1.4	
	845	0.10	0.0022	1.12	0.47	1.3	
	915	0.11	0.0023	1.33	0.47	1.2	
	985	0.12	0.0026	1.65	0.56	1.1	
Ti_3SiC_2 CG	50	0.02	0.00056	0.014	0.002	1.9[a]	≈ 1.5 assuming $N_{IKB}=0.3\times10^{18}$ m^{-3}
	100	0.04	0.001	0.047	0.008	0.9[a]	
	165	0.07	0.0011	0.078	0.02	0.3	
	200	0.09	0.0015	0.134	0.04	0.3	
	246	0.1	0.0016	0.18	0.067	0.2	
Graphite	36	0.0012	0.0017	0.048	0.01	9.3×10^{5}[a]	≈ 0.01 assuming $N_{IKB}=5\times10^{23}$ m^{-3}
	50	0.002	0.0024	0.091	0.025	4.7×10^{5}	
	63	0.0021	0.00345	0.161	0.041	6.2×10^{5}	
	75	0.0025	0.0046	0.256	0.065	5.8×10^{5}	

[a]These values are too high and must be due to the uncertainties in the calculation of ε_{IKB} at the low stresses.

U_{NL} in both microstructures is quite small. It follows that the main effect of the DPs is to shift the solid lines to the right. Said otherwise, at least for Ti_3SiC_2, the intercept along the x axis is a measure of DP activity. This conclusion should be valid for most KNE solids that tend to crystallize as thin plates for which $\lambda > 2\alpha$ insuring that the coefficient of the first term in Eq. (12) is always much smaller than that of the second term. Even in the case of the submicron-grained graphite (0.023 μm, see Table I) tested here, the ε_{DP} prefactor in Eq. (12) is an order of magnitude smaller than the ε_{IKB} prefactor. Needless to add, larger grain diameters, reduce the contribution of DPs to U_{NL} even further.

The solid lines in Fig. 4(b) are plots of the second term in Eq. (12) shifted to the right. These lines were generated as follows: First the slope of the line shown in Fig. 4(b) for FG Ti_3SiC_2 was used to calculate r, assuming 2α to be the value measured from image analysis, viz. 3 μm (Table I). Once r is determined, the slope of the CG Ti_3SiC_2 line is used to calculate the 2α in that microstructure. The value calculated, 11 μm, is in good agreement with the value of 2α determined from image analysis, i.e., 20 ± 16 μm (Table I).

For graphite the slope of the line is used to calculate r, assuming 2α to be that determined from XRD peak broadening (see the Appendix). It is gratifying that the values of r determined herein for both Ti_3SiC_2 and graphite ($\approx 11b$) are quite reasonable, and in the case of Ti_3SiC_2 bolstered by direct high-resolution TEM micrographs.[16] Needless to add, the results obtained are a weak function of r, and if better values of r are available in the future, they would have to be radically different than those chosen here to alter any of our conclusions. Along the same lines, the range of r values is limited; r can vary from a minimum of b to a maximum of b/γ_c. Higher values of r would result in imaginary energies [see Eq. (12), for example].

Once r and 2α were determined, 2β and N_K are calculated from Eqs. (5) and (7), respectively. These resulting values are listed in Table II as a function of stress. The average distance δ between IKBs (last column in Table II) was estimated assuming $\delta=(1/N_k)^{1/3}$, i.e., we assume the IKBs to be uniformly distributed. In all cases δ was found to be $>2\beta$.

2. High stress regime

Figure 4(a) plots Eq. (14) by fixing the strain exponent to 1.5 and varying the prefactor. The excellent agreement between theory (dashed lines) and experiment for all three solids over the entire stress range is gratifying and implies that the experimental results are consistent with our model. From the prefactors shown in Fig. 4(a) and Eq. (14), we calculate $N_k\alpha^3=3$ for FG Ti_3SiC_2, 22 for CG Ti_3SiC_2, and 0.5 for graphite. These values are quite reasonable and hover around 1 for the FG Ti_3SiC_2 and very fine-grained graphite samples. Assuming 2α for the FG, CG and graphite are, respectively, 3, 11, and 0.023 μm, the respective N_k's are 9×10^{17}, 1.3×10^{17} and 3×10^{23} m^{-3}. These numbers are in excellent

agreement with the same values obtained from Fig. 4(b) and listed in the last column in Table II.

To summarize, upon initial loading DPs in the soft grains result in an initial strain; the energy needed to form the pileups, however, is negligible compared to that needed to form the IKBs. It follows that the x axes intercepts of plots such as the ones shown in Fig. 4, yield information about dislocation pileups. The slopes of the lines, on the other hand, are related to IKB formation. Remarkably, therefore, an almost complete picture of the dislocation distributions, density, shapes, interactions, etc., can be determined from a single KNE solid stress-strain curve.

D. Dissipated energy

The energy dissipated per unit volume per cycle W_d which arises from the energy dissipated or friction due to dislocation motion is another important clue to what is occurring. If we assume that a dislocation loop sweeping an area $\pi\beta^2$, dissipates an energy per unit area, Ω, then in one cycle

$$W_d = 2N_k \pi \beta^2 \frac{2\alpha}{D}\Omega. \tag{15}$$

The factor of 2 comes because of the opening and closing of the IKB loops, i.e., loading and unloading that we assume are equal; the number of dislocation loops per IKB is $2\alpha/D$. Eliminating β using Eq. (5) yields

$$W_d = \frac{\pi \Omega N_k \alpha^3}{G^2 b \gamma_c}(\sigma^2 - \sigma_t^2), \tag{16}$$

where σ_t is a threshold stress below which no kinking occurs. It follows that if $\alpha^3 N_k$ is a weak function of stress, then a plot of W_d versus σ^2 should yield a straight line with a slope proportional to Ω and an intercept equal to σ_t^2. The excellent linear relationship shown in Fig. 5(a), indirectly confirms that to be the case. Note that if $\alpha^3 N_k$ were a function of stress, the exponent on the latter would be >2.

Multiplying the square of Eq. (9) by Eq. (16) yields

$$\Omega = \frac{2b(1-\nu)^2 U_{\mathrm{NL}}^2 W_d}{(\varepsilon_{\mathrm{NL}} - \varepsilon_{\mathrm{DP}})^3(\sigma^2 - \sigma_t^2)} \text{ for } \sigma > \sigma_t. \tag{17}$$

This is a powerful expression because it allows us to calculate Ω without knowing the atomistic details of the IKBs, i.e., N_k, α or β. It is important to note that this relationship assumes that W_d results from IKBs alone, which is a good assumption as long as the first term on the right-hand side of Eq. (13) is significantly smaller than the second. Figure 5(b) plots a log-log of the right-hand side of Eq. (17) as a function of applied stress for both Ti_3SiC_2 and graphite. The results show that Ω is a function of σ. As a first approximation it is not unreasonable to equate Ω/b to the critical resolved shear stress for dislocations gliding on the basal planes. This comment notwithstanding, it is hereby acknowledged that more

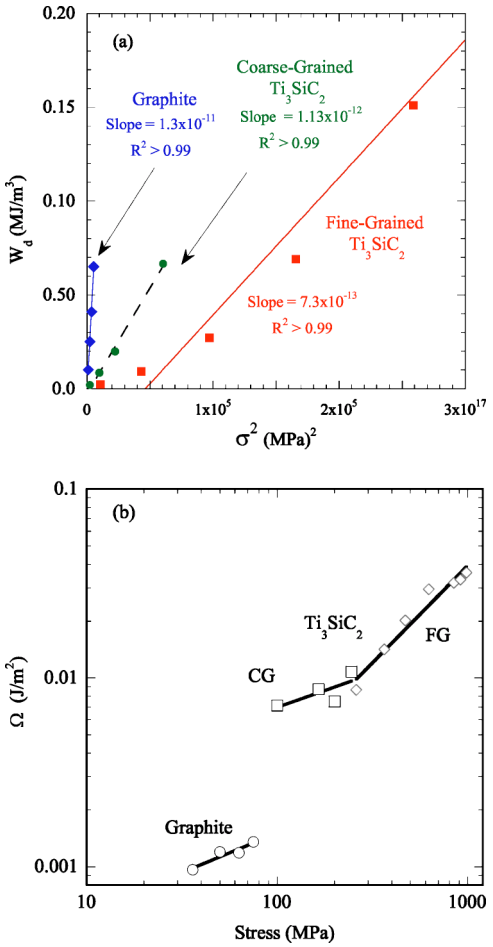

FIG. 5. (Color online) (a) Plot of W_d versus σ^2. The intercept of the lines with the x axis is equal to the threshold stress squared. (b) log-log plot of Ω vs maximum applied stress in each cycle.

work is needed to understand the relationship of Ω to other material properties and its dependence on the state of applied stress and microstructural variables. This work is ongoing.

Assuming Ω for graphite, FG and CG Ti_3SiC_2 to be $\approx$0.001, 0.02, and 0.01, respectively [Fig. 5(b)], $N_k\alpha^3$ can be calculated from Eq. (16) and the slopes of the lines shown in Fig. 5(a). At 16, 5, and 0.7, respectively, these values are in excellent agreement with the values calculated from Fig. 4(a) (see previous section). This independent check on the values of $N_k\alpha^3$ in the different solids lends even more credence to our model.

In principle, for an ideal system with monosized grains, $\sigma_t \approx \sigma_c$. One way to measure σ_t is from plots such as those shown in Fig. 5(a). Least squares analysis of these plots, results in σ_t's for graphite, CG and FG Ti_3SiC_2 of 23, 50, and 216 MPa, respectively. The corresponding values of σ_c calculated from Eq. (4) are 57, 130, and 250 MPa. This agreement has to be considered excellent given the many simplifying assumptions made and in view of the fact that σ_c is calculated using the average grain size, while σ_t is more dependent on the size of the largest grains in the distribution. Consistent with this notion is the fact that the agreement between σ_t for the FG material is better than the one for the CG with its wider grain size distribution. Note that the value

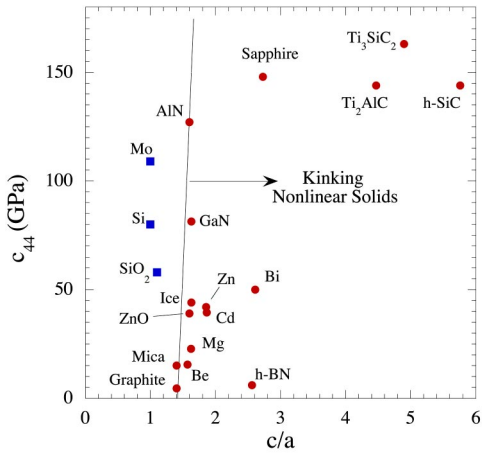

FIG. 6. (Color online) Plot of c_{44} versus c/a for non-KNE (solid squares) and currently known, or suspected KNE solids (solid circles). Solids that fall to the right of the near vertical line should be KNE solids.

of 2α used to calculate σ_t for the CG samples was 11 μm [i.e., that determined from the results shown in Fig. 4(b)]. If instead the 2α used is the one determined from the microstructure—which would be more relevant for calculating σ_t—the latter would be ≈100 MPa and thus in better agreement with experiment.

Two other factors can play an important role in reducing σ_t. First, the presence of potent nucleation sites for IKB formation. In the FS model the local stress required to nucleate a dislocation dipole is $G/30$. The presence of flaws and inclusions, for example, could act as potent stress concentrators that in principle should reduce σ_t.

Second is the loss of constraint. Since the formation of IKBs is essentially a buckling phenomenon, it is greatly enhanced when the grains are not constrained or confined. For example, KBs form preferentially at the corners of cubes,[8] and the mechanical properties are strong functions of the state of stress.[11,17] Similarly, the thresholds for the formation of IKBs under spherical nanoindentations are several times higher than the compressive strengths of the material.[2] We have also recently shown that porous Ti_3SiC_2 samples can dissipate more energy, on an absolute scale, than fully dense ones.[30] Given that the graphite tested here in ≈20 vol. % porous, the low σ_t value measured is not too surprising.

The excellent agreement between the widths of the grains obtained from Fig. 4(a) and the actual average width is quite gratifying and lends great credence to the FS model. The agreement observed between theory and experiment shown in Fig. 4(a) over the entire stress regime, with essentially no fitting parameters is even more remarkable considering the wide range—over three orders of magnitude—of grain sizes examined and the huge differences in bonding between Ti_3SiC_2 and graphite. In the former the bonds are a combination of covalent, metallic, and ionic,[31,32] in the latter the bonding between the basal planes is van der Waals.[27] Moreover, graphite is elastically hugely anisotropic, while Ti_3SiC_2 is quite isotropic.[2]

It is important to put the numbers calculated in Table II in perspective. Based on these results the total dislocation densities in the various samples are weak functions of stress. The response of the two Ti_3SiC_2 microstructures to stress are also different; the density of IKBs are between 4 and 5 times higher in the FG material. The IKBs in the FG material, however, are ≈3 times slimmer than in the CG samples and the main effect of increasing the stress is to increase β.

In Ti_3SiC_2 the spacing between dislocations D in a wall is 43 Å. The number of dislocation loops per IKB in the FG and CG samples is, respectively, 700 and 4670. Thus the total dislocation densities, in the FG and CG Ti_3SiC_2 microstructures, are $\approx 4\times10^{14}$ m^{-2} and $\approx 9\times10^{14}$ m^{-2}, respectively. These values are quite reasonable and fall in between those of well-annealed metal crystals and heavily cold-rolled ones.[28] Note these numbers do not include the DPs. They are also in good agreement with the value of 2×10^{14} m^{-2} determined from transmission electron microscope micrographs of bent areas in mica.[33]

In graphite, $D\approx 21$ Å and the average number of dislocations per IKB is 20, for a total dislocation density of $\approx 1\times10^{17}$ m^{-2}; a value that is roughly 20 times higher than typical values in heavily cold-rolled metals.[28] At this point it is not clear whether this result is plausible because of the nature of graphite, or is a reflection that some of the strain measured is a result of the fact that the samples were porous, i.e., due to sample compliance. We believe it is most likely a combination of both. Clearly more work is needed here.

Some final comments: We would like to point out that the fully reversible nature of the IKBs permits us to contemplate a heretofore impossible task: the development of a thermodynamic model that explicitly includes dislocations. We believe this paper is a first, but important step, in that direction. Furthermore as noted above, we postulated that a sufficient condition for a solid to be a KNE is solid is a high c/a ratio and/or a low c_{44}. Figure 6 plots the latter values for a number of solids, some of which are known to kink and others that are not. Based on this map it would appear that KNE solids lie to the right of the inclined vertical line and hence constitute a huge class of solids.

ACKNOWLEDGMENT

This work was supported by the Army Research Office (Grant No. DAAD19-03-1-0213).

APPENDIX

The room-temperature Young's, shear, and Poisson's ratios of Ti_3SiC_2 have been measured several times and it is now fairly well established that these values are, respectively, 340 GPa, 144 GPa, and 0.2.[34] The dislocations are perfect and mixed with a Burgers vector is 3.02 Å.[6,35] The dislocations arrange themselves in walls with alternating screw components.[6,35]

Typically the grains in Ti_3SiC_2 grow as thin hexagonal plates.[9,12] Given that the IKBs grow with their long dimension 2α parallel to the c axis, the relevant microstructural parameter is the *width* of the grains and not their length. Two Ti_3SiC_2 microstructures were tested; one in which the grains

were fine, equiaxed with an average thickness of 3 ± 1.5 μm and a narrow grain size distribution.[15] The average diameter of the grains λ was 8 ± 4 μm.[15] The second was coarse-grained with a wide grain size distribution. The average grain width was 20 ± 16 μm;[15] the average diameter, λ was 42 ± 39 μm.[15] The details of how these samples were made and their microstructures can be found elsewhere.[15]

In both cases, γ_c was calculated using Eq. (3) assuming τ_{loc} was $G/30$. β was calculated from Eq. (5). Note that the maximum value of r is b/γ_c or $\approx 15b$, before the term under the square root in Eqs. (4) and (8) becomes negative.

The graphite used was commercially available (Grade ISO-36, Toyo Tanso, USA, Troutdale, OR). The average grain, or crystallite size, determined from x-ray diffraction line broadening was 0.023 μm. Its density was 1.83 $\mathrm{Mg/m^3}$, which implies it was ≈20 vol.% porous.

Partials exist in graphite and their Burgers vector is 1.42 Å.[27] Young's modulus for polycrystalline graphite 10 GPa was determined from the slopes of the initial unloading portions of the stress/strain curves [Fig. 1(b)]. This value is typical for the polycrystalline graphite used here. The shear modulus was taken to be equal to c_{44} or ≈4.5 GPa.[27]

[1] M. W. Barsoum, T. Zhen, S. R. Kalidindi, M. Radovic, and A. Murugaiah, Nat. Mater. **2**, 107 (2003).
[2] A. Murugaiah, M. W. Barsoum, S. R. Kalidindi, and T. Zhen, J. Mater. Res. **19**, 1139 (2004).
[3] M. W. Barsoum, A. Murugaiah, S. R. Kalidindi, and T. Zhen, Phys. Rev. Lett. **92**, 255508 (2004).
[4] M. W. Barsoum, A. Murugaiah, S. R. Kalidindi, T. Zhen, and Y. Gogotsi, Carbon **42**, 1435 (2004)
[5] L. Farber, M. W. Barsoum, A. Zavaliangos, T. El-Raghy, and I. Levin, J. Am. Ceram. Soc. **81**, 1677 (1998).
[6] L. Farber, I. Levin, and M. W. Barsoum, Philos. Mag. Lett. **79**, 163 (1999).
[7] M. W. Barsoum, L. Farber, T. El-Raghy, and I. Levin, Metall. Mater. Trans. A **30**, 1727 (1999).
[8] M. W. Barsoum and T. El-Raghy, Metall. Mater. Trans. A **30**, 363 (1999).
[9] M. W. Barsoum and T. El-Raghy, J. Am. Ceram. Soc. **79**, 1953 (1996).
[10] M. Radovic, M. W. Barsoum, T. El-Raghy, S. Wiederhorn, and W. Luecke, Acta Mater. **50**, 1297 (2002).
[11] M. W. Barsoum, Prog. Solid State Chem. **28**, 201 (2000).
[12] T. El-Raghy and M. W. Barsoum, J. Am. Ceram. Soc. **82**, 2849 (1999).
[13] T. El-Raghy, M. W. Barsoum, A. Zavaliangos, and S. Kalidindi, J. Am. Ceram. Soc. **82**, 2855 (1999).
[14] M. W. Barsoum, M. Radovic, P. Finkel, and T. El-Raghy, Appl. Phys. Lett. **79**, 479 (2001).
[15] M. Radovic, M. W. Barsoum, T. El-Raghy, and S. Wiederhorn, J. Alloys Compd. **361**, 299 (2003).
[16] M. W. Barsoum and T. El-Raghy, Am. Sci. **89**, 336 (2001).
[17] M. W. Barsoum and M. Radovic, *Encyclopedia of Material Science and Technology*, edited by K. H. J. Buschow, R. W. Cahn, M. C. Flemings, E. J. Kramer, S. Mahajan, and P. Veyssiere (Elsevier Science, Amsterdam, 2004).
[18] R. A. Guyer and P. A. Johnson, Phys. Today **52** (4), 30 (1999).
[19] R. A. Guyer, K. R. McCall, and G. N. Boitnott, Phys. Rev. Lett. **74**, 3491 (1995).
[20] D. J. Holcomb, J. Geophys. Res. **86**, 6235 (1981).
[21] T. B. Anderson, Nature (London) **202**, 272 (1964).
[22] M. S. Paterson and L. E. Weiss, Nature (London) **195**, 1046 (1962).
[23] M. S. Paterson and L. E. Weiss, Geol. Soc. Am. Bull. **77**, 343 (1966).
[24] E. Orowan, Nature (London) **149**, 463 (1942).
[25] F. C. Frank and A. N. Stroh, Proc. Phys. Soc. London **65**, 811 (1952).
[26] J. B. Hess and C. S. Barrett, Trans. AIME **185**, 599 (1949).
[27] B. T. Kelly, *Physics of Graphite* (Applied Science Publishers, London, 1981).
[28] D. Hull, *Introduction to Dislocations* (Pergamon Press, Oxford, 1965).
[29] P. Duval, M. F. Ashby, and I. Anderson, J. Phys. Chem. **87**, 4066 (1983).
[30] Z. M. Sun, A. Murugaiah, T. Zhen, A. Zhou, and M. W. Barsoum (unpublished).
[31] N. Medvedeva, D. Novikov, A. Ivanovsky, M. Kuznetsov, and A. Freeman, Phys. Rev. B **58**, 16 042, (1998).
[32] B. Holm, R. Ahuja, and B. Johansson, Appl. Phys. Lett. **79**, 1450 (2001).
[33] I. A. Bell and C. J. L. Wilson, Tectonophysics **78**, 201 (1981).
[34] P. Finkel, M. W. Barsoum, and T. El-Raghy, J. Appl. Phys. **87**, 1701 (2000).
[35] B. J. Kooi, R. J. Poppen, N. J. M. Carvalho, J. Th. M. De Hosson, and M. W. Barsoum, Acta Mater. **51**, 2859 (2003).